Dry Reforming of Methane under Mild Conditions Using Radio Frequency Plasma

Devid, E.; Zhang, D.; Wang, D.; Ronda-Lloret, M.; Huang, Q.; Rothenberg, G.; Shiju, N.R.; Kleyn, A.W.

DOI
10.1002/ente.201900886

Publication date
2020

Document Version
Final published version

Published in
Energy Technology

Energy Technology
Generation, Conversion, Storage, Distribution
www.entechnol.de

Dry Reforming of Methane under Mild Conditions Using Radio Frequency Plasma

Edwin Devid, Diyu Zhang, Dongping Wang, Maria Ronda-Lloret, Qiang Huang, Gadi Rothenberg, N. Raveendran Shiju, and Aart W. Kleyn**

Dry reforming of methane (DRM) is a challenging process wherein methane reacts with CO_2 to give syngas. This reaction is strongly endothermic, typically requiring temperatures higher than 500 °C. Catalysts can be used, but the high temperatures (which are a thermodynamic requirement) often lead to catalyst deactivation. Herein, the reaction from another conceptual direction is approached, using low-power radio frequency inductively coupled plasma (RF-ICP). It is demonstrated that this system can give high conversions of methane and CO_2 at near-ambient temperatures. Importantly, the energy costs in this system are considerably lower compared with other plasma-driven DRM processes. Furthermore, it is shown that the yield of hydrogen can be increased by minimizing the C2 compound formation. The factors that govern the DRM process and discuss H_α emission and its influence on H atom recycling in the process are examined.

1. Introduction

The effects of climate change caused by greenhouse gases are numerous and include deglaciation, marine heatwaves, and threats to global biodiversity.[1–3] Carbon dioxide and methane are the most important anthropogenic greenhouse gases both by volume and by their contribution to the greenhouse effect. Ideally, society should stop emitting these gases completely, and hopefully this will be done in the future (see, e.g., the Sky scenario[4]). Meanwhile, we should focus research on approaches for minimizing the impact of methane and CO_2 and removing them from the atmosphere. This means that we also need chemical reactions that consume methane, without generating CO_2. One such possibility is the so-called dry reforming of methane (DRM: $CH_4 + CO_2 \rightarrow 2CO + 2H_2$). In this process, carbon dioxide and methane react to give syngas, a mixture of H_2 and CO, which can then be converted via Fischer–Tropsch synthesis into valuable hydrocarbon products.[5,6]

DRM is a strongly endothermic reaction, with $\Delta H^0 = 2.56$ eV or $+247$ kJ mol^{-1}. High temperatures (>500 °C) are needed to shift the equilibrium to the products side. However, such high temperatures mean very costly equipment and often cause catalyst deactivation via sintering and/or coking, e.g., see the studies by Ewbank et al. and Stroud et al.[7,8] Running the DRM process at lower temperatures is therefore a worthy scientific and technological challenge.

Plasma-based technologies for DRM have been widely studied.[9–11] DRM can be performed using plasma technology without the use of precious metal catalysts. Activation of carbon dioxide and methane molecules can be achieved in different ways through plasma: by thermal decomposition, using stepwise vibrational excitation, and electron collisions. For thermal plasma, thermal decomposition is the main process. In nonthermal plasma DRM, which is conducted at ambient temperatures, vibrational excitation is a more effective activation route.

The recent advances in DRM with plasma methods are summarized in several excellent reviews.[9–14] These indicate that DRM can be done with many plasma methods, giving conversions of around 40% at an energy cost range between 1.2 and 200 eV per molecule. Energy efficiencies of DRM conducted through plasma technologies are difficult to determine, because during plasma-driven DRM, a variety of species and products are generated, including H_2, CO, CH_3•, H_2O, C_2H_2, C_2H_4, C_2H_5•, C_2H_6, C_3H_8, and C_4H_{10}. The wide product distribution affects the definition of energy efficiencies. Thus, plasma-based DRM processes are typically expressed in terms of "energy cost," i.e., the amount of energy consumed by the DRM process in unit of eV per converted molecule.[11] The energy cost (eV per molecule$_{conv.}$) is therefore

Dr. E. Devid, D. Zhang, Dr. D. Wang, Dr. Q. Huang, Prof. A. W. Kleyn
Center of Interface Dynamics for Sustainability
Institute of Materials
China Academy of Engineering Physics
596 Yinhe Road 7th section, Chengdu, Sichuan 610200, P. R. China
E-mail: ejdevid@outlook.com; a.w.kleijn@contact.uva.nl

D. Zhang
Leiden Institute of Chemistry
Leiden University
Einsteinweg 55, 2333 CC Leiden, The Netherlands

M. Ronda-Lloret, Prof. G. Rothenberg, Dr. N. R. Shiju
Van 't Hoff Institute for Molecular Sciences
Faculty of Science
University of Amsterdam
P.O. Box 94157, 1090 GD Amsterdam, The Netherlands

Dr. Q. Huang
School of Optoelectronic Engineering
Chongqing University of Posts and Telecommunication
Chongqing 400065, P. R. China

The ORCID identification number(s) for the author(s) of this article can be found under https://doi.org/10.1002/ente.201900886.

DOI: 10.1002/ente.201900886

$$\frac{\text{Power(kW)} \times 60(\text{s min}^{-1}) \times 24.5(\text{L mol}^{-1}) \times 6.24 \times 10^{21}(\text{eV kJ}^{-1})}{\text{flowrate(L min}^{-1}) \times \chi_{\text{total}} \times 6.022 \times 10^{23}(\text{molecule mol}^{-1})} \quad (1)$$

Recently, several studies were published on DRM using dielectric barrier discharges (DBDs).[15–18] Good yields are reported, but only when a catalyst is inserted in the DBD reactor. The study by Ray et al. demonstrates that without a catalyst DRM yields by plasma only are below 10%. Herein, we demonstrate much higher product yields without using a catalyst, applying radio frequency inductively coupled plasma (RF-ICP).[19] RF-ICP has several advantages that makes it suitable for DRM: 1) RF allows to generate nonthermal plasma at low pressures (i.e., 1–10^3 Pa). This is useful to drive the DRM process in a controlled way, without yielding a very wide variety of products. 2) RF plasma can be produced at low frequencies, ranging between 1 and 100 MHz. In this range, a large plasma volume of approximately the entire size of the plasma reactor can be generated. This ensures that the DRM process is driven in a fully homogeneous plasma. It is especially relevant for industry as it improves the scalability. 3) RF plasma's energy efficiency can be optimized through an impedance matching network. By matching the impedance of the RF power generator to the RF plasma discharge one can minimize the reflected RF power to the plasma reactor. Theoretically when optimized coupling can be obtained between the plasma and the RF field, the energy efficiency of plasma-based selective heating can be up to 90%.[20,21] 4) The electrodes for generating RF-ICP are located outside the plasma reactor (see also Experimental Section). This is advantageous for the plasma-driven DRM process, as the nonthermal DRM plasma will not be contaminated by the metal electrodes. 5) Finally, RF-ICP allows to analyze the DRM process in a simple, accessible, noninvasive way, such as mass spectrometry, optical emission spectroscopy, and laser-based methods.

Despite its potential, very little is reported on DRM by RF-ICP. Mozetic et al. published an extensive article on activation of CH_4 by RF-ICP.[22] They showed that the main reaction products are hydrocarbons, carbon deposits, and H_2. The relative abundance of each product strongly depends on the plasma conditions. Increased energy deposition in plasma leads to more hydrocarbon formation. Patino et al. also conducted studies on DRM with RF-ICP. The study focuses strongly on data analysis and experiment selection.[23] In addition, they focused on steam reforming, for which they obtain high syngas yields. However, for DRM, their yields are very low. Chen et al. studied the pyrolysis and oxidation of CH_4 in a He RF discharge. The authors complement their work with extensive kinetic modeling.[24] Other recent works have used radio frequency capacitively coupled plasma (RF-CCP).[25–30] These systems are similar to DBD.[11] The work with RF-CCP is more focused on dissociation of CH_4 and carbon deposition than on DRM. In CCP-based plasma setups, the electrodes are inside the reaction vessel where the electrodes get quickly contaminated. External coils, as used in RF-ICP, are preferable for DRM.

Recently, Ray et al. published in this journal work on performing DRM in an improved DBD reactor with catalysts and the possibility of heating them up thermally to obtain higher yields of syngas.[19] Confirming earlier studies, Ray et al. demonstrate that the energy cost of performing DRM by DBD both with or without catalysts remains very high (about five times the thermal equilibrium limit).[19] In our work, we will compare the DRM performance of the improved plasma-enhanced temperature DBD of Ray et al. with our plasma-only RF-ICP reactor.

Another way to produce valuable hydrocarbons from methane without syngas involves the partial oxidation of methane to methanol. Using plasma technology also, this route is available.[31,32]

Our work builds upon the work on methane activation by Mozetic et al. We utilize lower power, flow, and pressure and discover that C2 compound formation decreases together with increased formation of H_2. This is a relevant finding for DRM. In addition, we show that DRM can be conducted in a RF-ICP setup with very high conversions and can compete on energy cost with other types of plasma-driven DRM processes. Finally, we discuss the observation of water formation and its influence on hydrogen atom recycling in the process.

2. Results

2.1. Quadrupole Mass Spectrometry Analysis of Activation of Pure CH_4

Quadrupole mass spectrometry (QMS) allows us to observe in real time both qualitatively and quantitativly the species formed in plasma at low pressures. Details of the analysis are reported in the Experimental Section.

Figure 1a shows the relative concentrations of product species from pure CH_4 reforming in RF-ICP and the carbon balance at different input powers. For decomposition of pure CH_4, the product's H/C ratio should be 4 (irrespectively of the RF power). In fact, this ratio increases from 4 at 0 W to 4.6 at 150 W. This indicates a loss of carbon by deposition of a carbonaceous film on the reactor wall. From the carbon balance plotted in Figure 1a (calculated as given in the caption and following the study by Ray et al.[19]), it is shown that with increasing power the loss of carbon behaves linearly. With increasing specific energy input (SEI), more CH_4 dissociates into H_2 and C, where carbon gets deposited at the reactor walls.

A direct in situ spectroscopic analysis of this film is not possible. However, we see the formation of a yellow film inside the reactor tube after prolonged operation. In previous studies, we measured the electron temperature. In the present arrangement, this was not possible.[20,33] However, based on our results, we estimate it to be between 2 and 5 eV. This means that direct electronic excitation of CO_2 is unlikely.

Our results show that RF-ICP can effectively activate methane molecules. The main products of CH_4 reforming were hydrogen and C2 hydrocarbons. Increasing the power, the conversion of methane increased up to 60% (Figure 1a,b). The yields of H_2 and C2 hydrocarbons sharply increased below 50 W. With a further increase in power, H_2 yield increased steadily and the C2 yield stabilized. The highest concentration was for H_2 with 50% (at 150 W) of all gaseous products (Figure 1a), and the total H_2 yield over H-containing products was 35% at 150 W. The energy cost for CH_4 reforming follows here a linear trend as a function of the input power, which is lower compared with most plasma-based

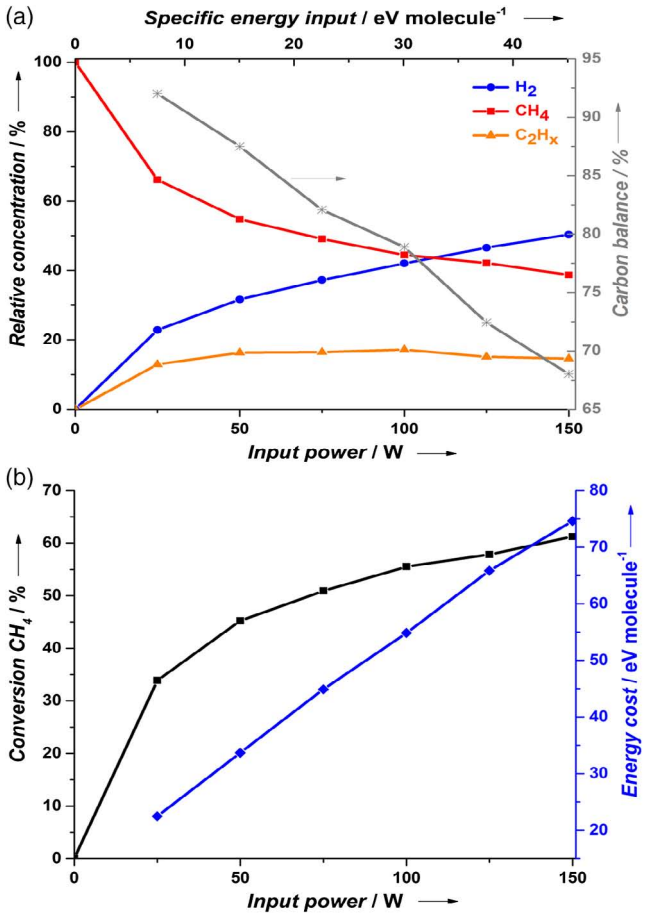

Figure 1. a) Relative molecular concentration of effluent gas from pure CH_4 reforming at different input powers. On the right *y*-axis the carbon balance is shown (%) where the ratio = $(CH_{4\ out} + 2 \times C_2H_{x\ out})/(CH_{4\ in}) \times 100\%$. Reaction conditions: feed: CH_4; flow: 50 sccm; and pressure: 44 Pa. b) Conversion of CH_4 as a function of input power. The energy cost for pure CH_4 reforming by RF-ICP is shown on the right (blue colored) *Y*-axis. The energy cost is defined as power (kW) × 60 ($s\ min^{-1}$) × 24.5 ($L\ mol^{-1}$) × 6.24×10^{21} ($eV\ kJ^{-1}$) divided by (flow rate ($L\ min^{-1}$) × $\chi_{Total} \times 6.022 \times 10^{23}$ ($molecule\ mol^{-1}$)). The reaction conditions: feed: CH_4; flow: 50 sccm; and pressure: 44 Pa.

DRM studies conducted in DBD reactors.[11,19] Thus, RF-ICP is more energy efficient than DBD for CH_4 reforming.

Previously, we could not determine which fraction of the RF power is absorbed by the plasma.[20] In the case of RF plasma etchers, the energy efficiency can be up to 90%.[21] Therefore, our numbers for energy input into the plasma should not be seen as the ultimate obtainable by RF. Assuming that the RF power emitted into the coil is entirely absorbed by the plasma, we can determine the SEI into CH_4. The corresponding SEI is given on the top axis of Figure 1a. A power of 150 W corresponds to an SEI of 46 eV/CH_4. The corresponding energy efficiency depends on the specific reaction. The heat of formation of CH_4 from C(solid) and H_2 is 0.77 eV. The heats of formation of C_2H_x vary from 2.36 to −0.87 eV per molecule.

We also studied the pressure dependence of the methane conversion at a power of 150 W and pressures from 50 to 200 Pa at the same flow of 50 standard cubic centimeter per minute (herein: sccm) (data not shown). We observe that the conversion of CH_4 decreases with increasing pressure. This is a factor of 1.5 over the pressure range mentioned.

2.2. QMS Analysis of Activation of Mixtures of CH_4 and CO_2

The DRM process is activated through a nonthermal plasma generated by RF-ICP (see also the Experimental Section). QMS allows us to real time probe in a nonevasive way both qualitatively and quantitatively the low-pressure effluent gases from our plasma reactor. **Figure 2**a shows the observed unreacted reactants (see black line on mass spectrum) and the formed species during plasma-driven DRM at 75 W (see blue line). Figure 2a shows clearly that CH_4 and CO_2 are converted by plasma only into H_2 and CO. To extract quantitative information from QMS, a calibration is performed for each gas species (such as H_2, CO, CH_4, CO_2, and O_2) that requires to be identified in the plasma reactor. The calibration and analysis are described in the Experimental Section.

The feed fraction of $CO_2/(CH_4 + CO_2)$ is one of the key factors affecting the DRM.[10,34–36] Figure 2b shows the relative molecular concentrations derived from QMS signals of effluent gas from mixed CH_4/CO_2 reforming in RF-ICP at different $CO_2/(CH_4 + CO_2)$ fractions. Detection of H_2O is difficult, because it is efficiently absorbed by the system walls. This is confirmed by the observation that it can take more than 1 h to bring the H_2O level in the residual gas back to a low level of a few Pa. For the C_2H_x contribution, we use the same method described previously for the pure CH_4 feed.

To test the data consistency, we analyzed the H/C and O/C ratios. For a 1:1 mixture of CH_4 and CO_2, about 20% of the C atoms are "missing," which indicates that they are probably deposited on the system walls. In the case of a CO_2-rich plasma, O/C reaches a below the expected value of 2 by up to 30%. We infer that both C and O can be adsorbed by the walls of the pumping system and potentially lead to H_2O, via the presence of H, that also can be absorbed on the system walls and escape detection.

As shown in Figure 2b, the main products of the DRM in RF-ICP are H_2, CO, O_2, and C2 hydrocarbons. Changing the ratio of CO_2:CH_4 significantly alters the ratio of the products. Increasing the proportion of CO_2 from 0% to 70%, the C2 hydrocarbons decrease, whereas the H_2 concentration remains almost same (Figure 2b). In plasma, pure CO_2 is decomposed into CO and O_2. For pure CO_2, the O_2 relative concentration (17%) is almost 50% of that of the CO concentration (40%). With a small amount of CH_4 (0.8 $CO_2/(CH_4 + CO_2)$) added, the O_2 decreased from 17% (at 100% CO_2 feed) to 7%. This is attributed to the rapid reaction of CH_4 with O to produce H_2O or OH, both of which are not detected by QMS. In addition, O_2 varies slightly between experiments with low $CO_2/(CH_4 + CO_2)$ fractions. Most likely, it depends on the amount of H_2O adsorption on the system walls.

The yields and selectivity of H_2 and CO are shown in Figure 2c. The H_2 yield with respect to the incident H atoms (in CH_4) increases with CO_2 content in the flow. The CO yield is basically constant between 40% and 55% at the $CO_2/(CH_4 + CO_2)$ feed

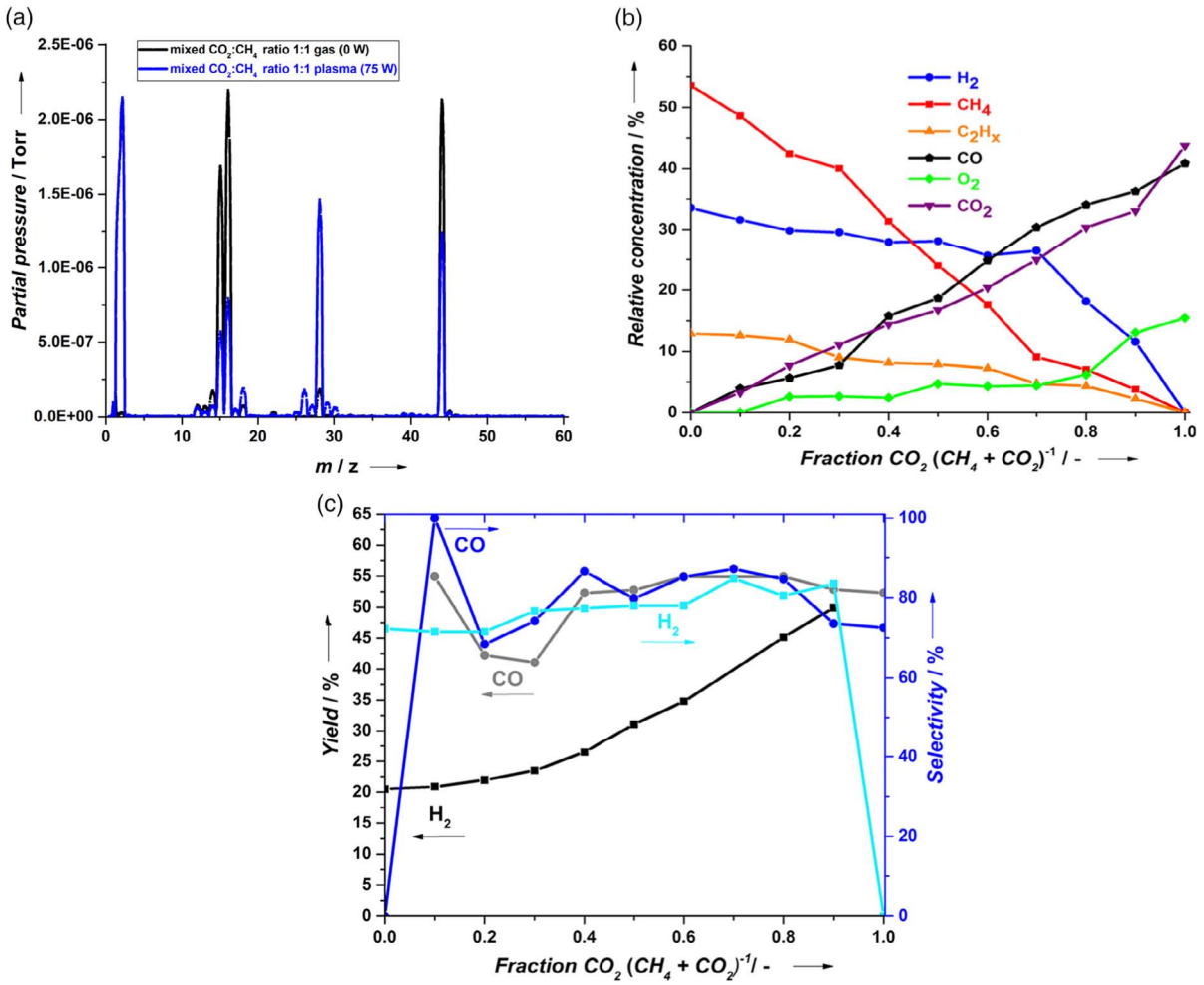

Figure 2. a) Mass spectra of real-time observed mixed CO_2:CH_4 (1:1) gas effluent at 0 W (see black line) versus the same mixed CO_2:CH_4 (1:1) gas now turned into plasma (see blue line). Reaction conditions: Total feed is 50 sccm; input power: 75 W; pressure mixed CO_2:CH_4 (1:1) gas effluent at 0 W is 36 Pa. Pressure mixed CO_2:CH_4 (1:1) plasma effluent at 75 W is 40 Pa. b) Relative molecular concentrations of effluent gas from mixed CH_4/CO_2 reforming at different $CO_2/(CH_4 + CO_2)$ fractions. Reaction conditions: feed: CH_4 and (or) CO_2; input power: 75 W; total flow: 50 sccm; and pressure: 50 Pa. c) H_2 and CO yields as a function of the fraction $CO_2/(CH_4 + CO_2)$. The H_2 yield is defined as $2 \times H_2$ intensity divided by the total H intensity detected in the products ($H_2 + CH_4 + C_2H_x$). The CO yield is defined as the CO intensity over the sum of CO and CO_2 intensities. The H_2 selectivity is defined as the H_2 intensity divided by the sum of the product ($H_2 + C_2H_x$) intensities converted from CH_4. The CO selectivity is defined as the CO intensity divided by the sum of the products ($CO + O_2$) intensities converted from CO_2. Reaction conditions: feed: CH_4 and (or) CO_2; input power: 75 W; total flow: 50 sccm; and pressure: 50 Pa.

fractions 0.4–0.9. The reason for the appearance of a dip in the CO yield around 0.2 and 0.3 feed ratio is not known. The selectivity of H_2 increases from 72.3% to 83.5% when the fraction $CO_2/(CH_4 + CO_2)$ reaches unity.

The selectivity of CO peaks to 100% at the fraction 0.1. Beyond the fraction 0.1, the selectivity shows small fluctuations around 80%. Higher fractions $CO_2/(CH_4 + CO_2)$ show that the presence of more CO_2 in the mix enables the increasing selectivity and yield of H_2. The decrease in CH_4 in the mix shows that the decomposition of CH_4 affects little to none the selectivity and yield of CO.

Figure 3a shows the power dependence of the relative concentrations derived from QMS signals of the effluent gas from mixed CH_4/CO_2 reforming in RF-ICP at $CH_4/CO_2 = 1$. Figure 3a also shows the carbon balance of the mixed CH_4/CO_2 reforming in RF-ICP at $CH_4/CO_2 = 1$. With increasing SEI, the decrease in carbon balance behaves nonlinearly. At higher input powers, a steady state is reached in carbon loss. The presence of a CO_2 feed at $CH_4/CO_2 = 1$ enables to limit the carbon loss. Presumably the carbon from the dissociated CH_4 reacts with the atomic O atoms from the dissociated CO_2. This observation corresponds with the steady-state concentration of O_2 in Figure 3a that explains why the O_2 concentration does not increase further with increasing power beyond 75 W.

RF-ICP grants here the combination of carbon and atomic oxygen into CO, thereby increasing further the yield of CO compared with the yield of C_2H_X molecules.

Measurement conditions are similar to those previously discussed in Figure 2. The H/C and O/C ratios were analyzed to test the consistency of the data. For a 1:1 mixture of

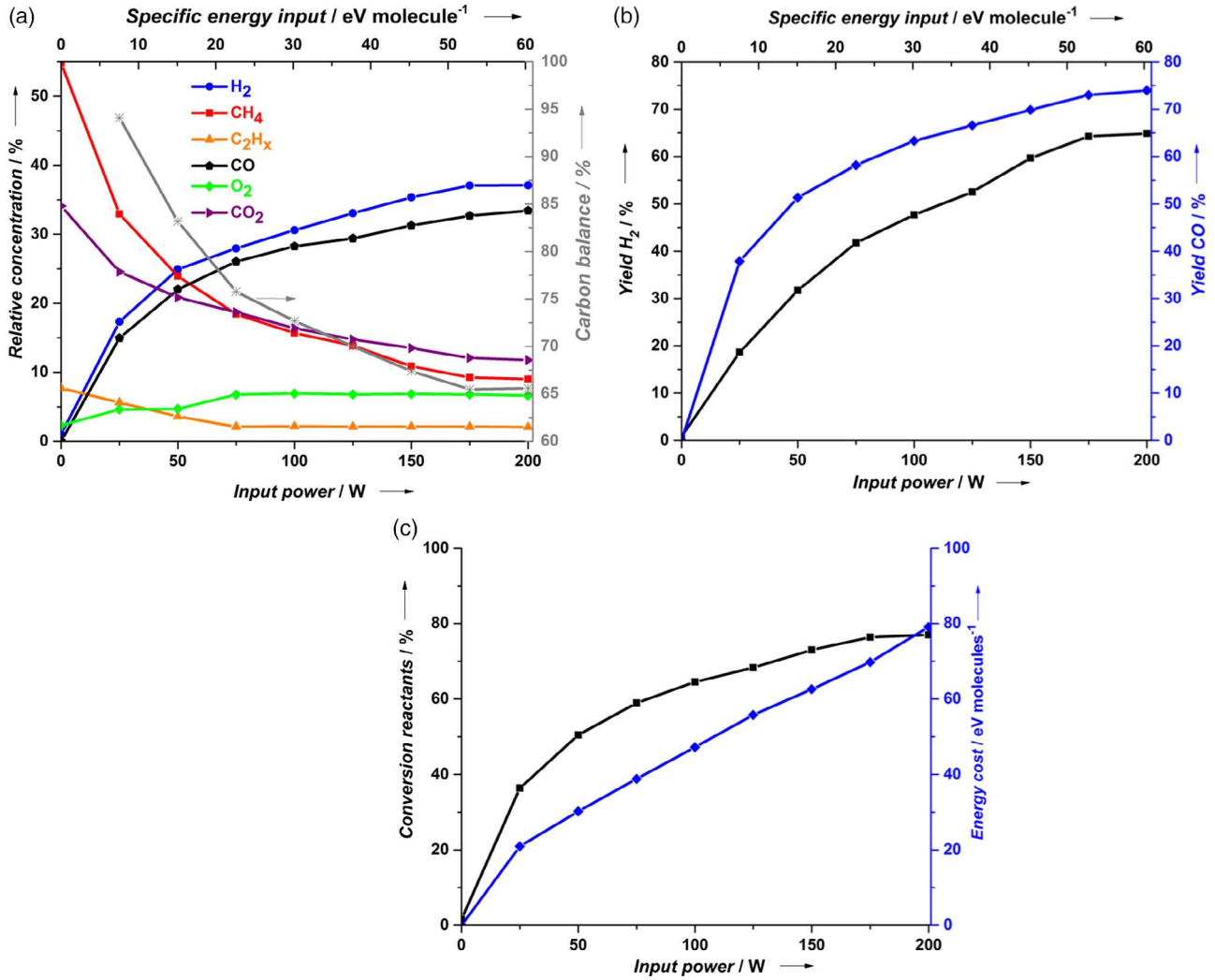

Figure 3. a) Relative molecular concentrations of effluent gas from CH_4 and CO_2 reforming at a fixed CH_4/CO_2 ratio of unity as a function of input power. The right ordinate shows the carbon balance (%) where the ratio = $(CH_{4\ out} + CO_{2\ out} + 2 \times C_2H_{x\ out})/(CH_{4\ in} + CO_{2\ in}) \times 100\%$. Reaction conditions: equal feed ratio: CH_4 and CO_2; total flow: 50 sccm. b) The H_2 and CO yields as functions of input power and SEI. Reaction conditions: equal feed ratio CH_4 and CO_2; total flow: 50 sccm. c) Total conversion of reactants and the energy costs of effluent gas from mixed CH_4/CO_2 reforming at a fixed CH_4/CO_2 ratio of unity as a function of input power. Reaction conditions: equal feed ratio: CH_4 and CO_2 and total flow: 50 sccm.

CH_4 and CO_2, about 20% C atoms is "missing" irrespective of power. The O/C ratio can deviate from the ideal value 1 by more than 20%. Formation of H_2O is likely under these conditions.

The yields of H_2 and CO are shown in Figure 3b. Both H_2 and CO yields gradually increase with increasing power. At 200 W, H_2 yield is 65% and CO yield is 74%.

The total conversion of mixed CH_4/CO_2 (1:1) reaches 77% (200 W) by plasma-only RF-ICP (see Figure 3c). This value is better than the absolute conversion of CH_4 and CO_2 of Ray et al., respectively, 68% and 65% obtained in their plasma-assisted thermal DBD reactor with the addition of their best-performing catalyst 15% Ni/Al_2O_3.[19] Without the catalyst, Ray et al. obtain a maximum yield for both CO ad H_2 of 10%. In this case, power and flow are lower so a good comparison cannot be made. DRM driven by RF-ICP plasma only has the advantage that no catalysts are required to obtain high syngas yields, and so there is no need to find suitable catalysts resistant to coke formation.

Figure 3c shows that the energy cost of DRM at a CO_2:CH_4 ratio of 1:1 is here lower than the energy cost of reforming CH_4 only (Figure 1b). RF-ICP on CO_2:CH_4 mixed ratios provides energy costs comparable with DRM studies conducted by atmospheric pressure glow discharge (APGD) (**Table 1**).[11]

Table 1 shows the total conversion and energy cost for multiple different plasma-driven DRM processes (originating from the study by Snoeckx and Bogaerts[11]). Our RF-ICP-driven DRM process reaches a total conversion range of 0–77% (from 0 W to 200 W) and an energy cost range of 0–79 eV per molecule (from 0 W to 200 W). Comparing our performance ranges with the ones from Table 1, we observe that our RF-ICP-driven DRM outperforms microwave (MW) and DBD-operated DRM processes. The DRM processes operated by DBD[37–39] reach

Table 1. Total conversion versus energy cost of the DRM process by different plasma systems.[11,37–44]

	Gliding Arc	APGD	Spark	Nanosecond pulse discharge	Corona discharge	MW	DBD
Total conversion [%]	3–44	36–88	7.5–96	0–64	14–90	50–73	0–85
Energy cost [eV per molecule]	1–50	0.9–60	3.2–10.6	3–100	4.2–30	120–400	12–600

close to the total conversion and energy cost of our RF-ICP-driven DRM performances. Furthermore, our RF-ICP-driven DRM performances reach closely the performances of APGD.[40,41]

Finally, RF-ICP-driven DRM reaches total conversions similar to corona and spark-driven DRM. But the energy cost with our RF-ICP is, respectively, about a factor 2 and factor 5 higher. However, we note that the efficiency of our RF-ICP system is not optimized and that better efficiencies should be obtainable using RF-ICP. By tuning the mixed ratios of the reactants, the energy cost of DRM by RF-ICP can be further changed and optimized.

2.3. Optical Emission Spectra Analysis of Activation of Mixtures of CH_4 and CO_2

We measured the optical emission spectra (OES) for CH_4/CO_2 mixtures as a function of composition (**Figure 4**) and as a function of input power for an equimolar mixture. In the analysis, we focus on the emission of the CO $b^3\Sigma^+$ state, OH, O atoms, and H atoms. To compare the emission intensity at different compositions of the mixture, the peaks of H_α and the 0-0, 0-1 transition of CO ($b^3\Sigma^+ - a^3\Pi$) system are integrated (**Figure 5**).

Figure 4 and **6** show CO vibrational progressions that do not exhibit large vibrational excitations, such as the ones we previously observed for CO_2 plasma diluted by Ar.[20] The CO emission spectrum changes when tuning the CH_4/CO_2 ratios (Figure 4). The emission from CO and O atoms will dominate the OES in a pure CO_2 feed. As the proportion of CH_4 in the feed is increased from 0% to 10%, the emission peak of O atoms decreased drastically, and an OH emission band ($A^2\Sigma^+ - X^2\Pi$) appears in the 300–320 nm region. In addition to the emission from OH, also, a large H_α emission intensity was observed at 10% CH_4 in the mixed feed CH_4/CO_2 case rather than in pure CH_4 which has highest H/C ratio and H_2 yields.

The integrated intensities of two CO lines, two O atom lines, and H_α emission are shown in Figure 5, as a function of the relative CO_2 content of the feed. The CO emission shows a linear increase with CO_2 content, very similar to the CO yield observed by QMS (Figure 2b). The linear increase seen in both QMS and OES of the CO signal confirms that the decomposition of the mass 28 signal to C_2H_x and CO is done correctly. The QMS data show no leveling off of the CO signal, as shown for CO emission in Figure 5. We attribute this to change in plasma parameters at the highest CO_2 fraction, leading to a smaller electronic excitation of CO.

The O atom signal in Figure 5 shows a marked increase at the highest CO_2 content (>0.7). The H_α emission shows a peak at the CO_2 content of 0.9, where the number of H atoms introduced by CH_4 is already very low.

The power dependence of the OES is shown in Figure 6a,b where the same spectral regions are shown as in Figure 4. We see that the emission of H_α and 0-0, 0-1 transition of CO ($b^3\Sigma^+ - a^3\Pi$) system increase as the power increases. For equimolar mixtures, no O atom emission is observed. In addition, the CO_2^+ doublet is observed, centered at $\lambda = 288.3$ nm and $\lambda = 289.6$ nm. OH emission is also observed (especially at a higher power) for the equimolar mixture. The line integrated intensities are shown in **Figure 7**. The trends observed are very similar to what is observed by the QMS intensities in Figure 3.

Figure 6b shows that the emission of H_α during RF-ICP-driven DRM intensifies by increasing the power to 75 W. Above 75 W, the emission of H_α levels off as a function of the input power. This indicates that RF-ICP-driven DRM enables easy excitation of hydrogen into H_α. RF-ICP offers an easy and accessible way to yield high levels of H_α.

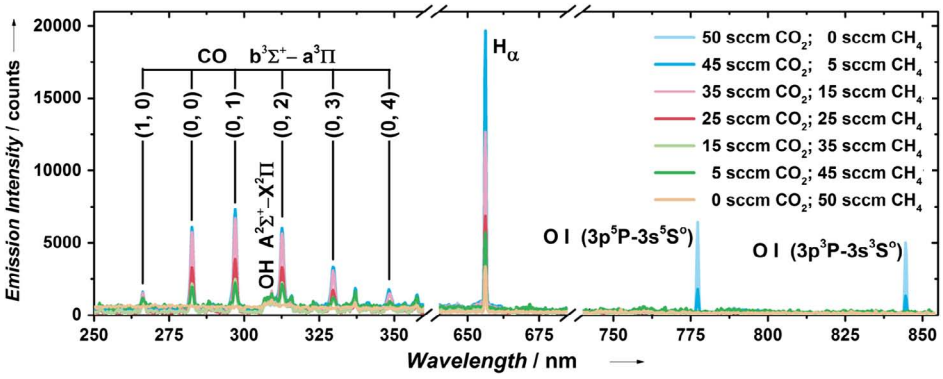

Figure 4. OES from CO_2 and CH_4 reforming at different CH_4/CO_2 ratios. Reaction conditions: feed: CH_4 and (or) CO_2; input power: 75 W; total flow: 50 sccm; and pressure: 50 Pa.

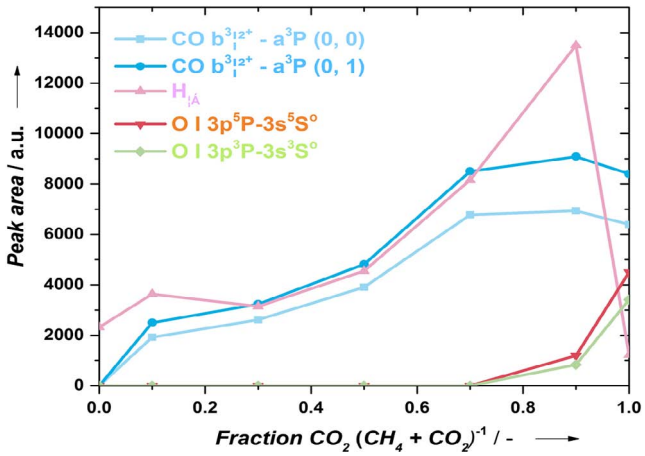

Figure 5. Integrated emission intensity of 0-0, 0-1 transition of CO ($b^3\Sigma^+ - a^3\Pi$) system, H_α, and O I ($3p^5P \rightarrow 3s^5S^\circ$, $3p^3P \rightarrow 3s^3S^\circ$). Reaction conditions: input power: 75 W; total flow: 50 sccm; and pressure: 50 Pa.

3. Discussion

3.1. Activation of Methane

For a comparison to our DRM experiments, we conducted the RF-ICP-induced activation of pure methane. With increasing SEI, we observed an increasing dissociation. At the highest power (150 W, SEI = 45.71 eV per molecule), 60% of CH_4 was converted into H_2, C_2H_x, and C deposit. Conversion efficiencies of CH_4 are very significant at these power levels. There are very few similar studies using RF-ICP. The most comparable work is the study by Mozetic et al.[22] These authors also studied pure CH_4 discharges. However, their setup is different, as it contains a special after-glow chamber connected to the plasma chamber via a small orifice. Moreover, the RF power used in their study (≈1200 W) is six times higher than what we use here. Our system gives a higher conversion, which can be attributed to the lower operating pressure and possibly the absence of a buffer chamber. Comparing our results with those of Mozetic et al., we conclude that methane conversion of more than 50% can be obtained at lower power levels and pressures as well. This indicates that efficient DRM can be expected with RF-ICP, as we discuss n the following sections.

3.2. Activation of Mixtures of CH_4 and CO_2

The product concentration of a CH_4/CO_2 mixture is shown in Figure 2b as a function of the CO_2:CH_4 feed composition. As expected, the CH_4 signal linearly decreases with the $CO_2/(CH_4 + CO_2)$ fraction, whereas the CO_2 relative concentration linearly increases. Also, the CO concentration linearly increases. The CO yield is constant at 48% at 75 W. Figure 2c shows that the CO yield is nearly constant as a function of feed composition. This implies that the conversion of CO_2 into CO is independent of feed composition. Figure 3b shows that the CO yield increases with power, where even values of 75% CO yield can be reached at 200 W. The CO yield in DRM at 200 W is higher than what we measured for pure CO_2. The limited yield

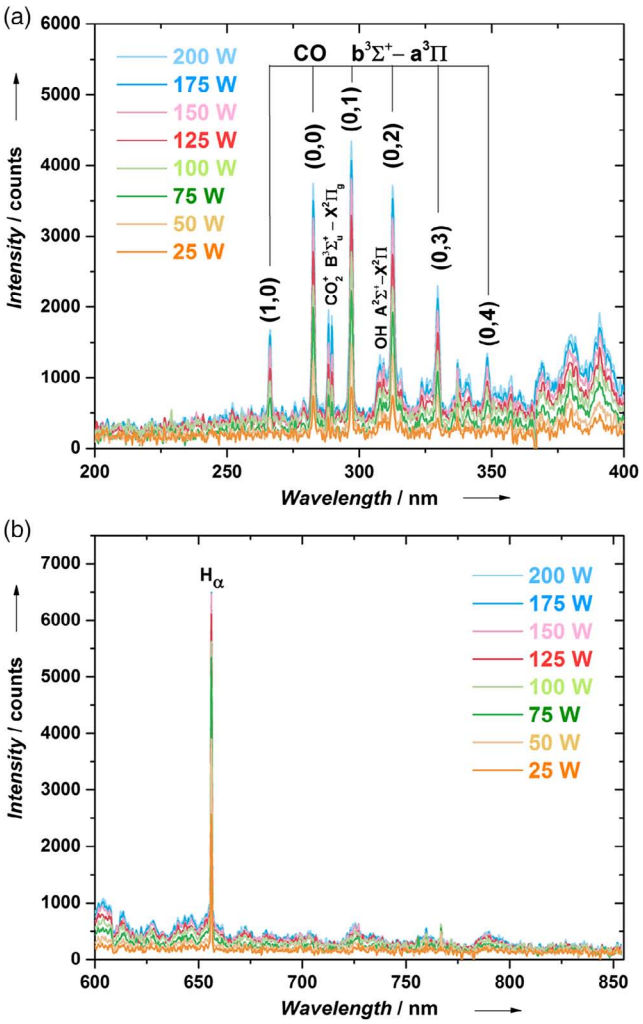

Figure 6. a) OES from CO_2 and CH_4 reforming in RF-ICP at different input powers in two spectral ranges. Reaction conditions: feed: 25 sccm CH_4 and 25 sccm CO_2 and pressure: 39 Pa. b) OES from mixed CH_4/CO_2 reforming in RF-ICP at different input powers in two spectral ranges. Reaction conditions: feed: 25 sccm CH_4 and 25 sccm CO_2 and pressure: 39 Pa.

in pure CO_2 plasma is attributed to recombination of the reaction products CO + O back to the reactant CO_2, e.g., see the studies by Yin and coworkers.[45–47] RF-ICP-driven DRM enables the suppression of the reverse reaction.

The product H_2 in Figure 2b is not proportional to the fraction of CH_4 in the feed. It is almost constant at a level 27–33% and decreases at $CO_2/(CH_4 + CO_2)$ fractions above 0.7. As a consequence, the H_2 yield (Figure 2c) increases as a function of $CO_2/(CH_4 + CO_2)$ fraction. Increasing power, as shown in Figure 3b, increased the H_2 yield to almost 75%. This shows that the formation of syngas has a high probability. Thus, RF-ICP-driven DRM is an efficient and clean way to produce syngas. The energy cost between CH_4 reforming (Figure 1b) versus mixed CO_2:CH_4 reforming (Figure 3c) shows significant differences, especially when compared with the total conversion. RF-ICP reforming of mixed CO_2:CH_4 ratios achieves lower energy costs while

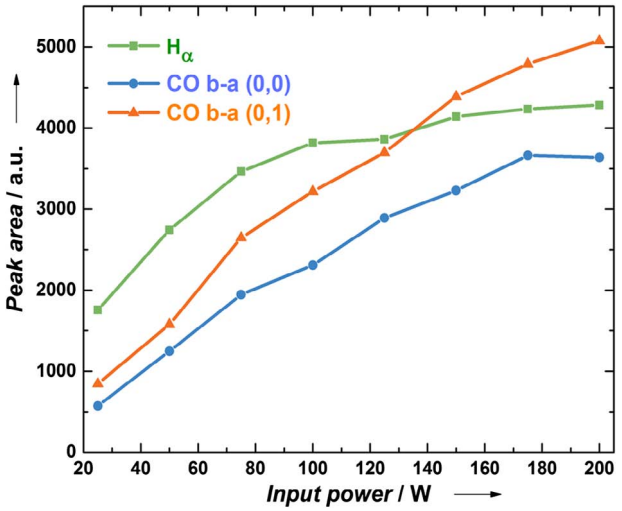

Figure 7. Integrated emission intensity of 0-0, 0-1 transition of CO ($b^3\Sigma^+ - a^3\Pi$) system and H_α as a function of input power. Reaction conditions: feed: 25 sccm CH_4 and 25 sccm CO_2 and pressure: 39 Pa.

significantly increasing both H_2 and CO yields at low powers (Figure 3b). Optimizing the coupling of power into the plasma will be a next step in this work to further enhance the energy efficiency.

The CO optical emission intensity shows a similar trend with QMS regarding the mass 28 peak. This indicates that most of the product under CO_2 feed is CO. In addition, the H_2 yield is very high. This indicates that syngas can be produced by DRM through RF-ICP at a low specific energy.

3.3. H_α Emission

A most remarkable observation in OES is the strong H_α emission at high $CO_2/(CH_4 + CO_2)$ fractions in the feed, as shown in Figure 4 and 5. The highest optical emission intensity of H_α was achieved at 90% CO_2 in the feed, where relatively few H atoms are introduced into the discharge. Nevertheless, the strong H_α emission indicates that a high number of H atoms is present in the plasma. We attribute this signal to the presence of H_2O in the discharge, preferably for a high CO_2 content. H_2O cannot be easily detected in the discharge by QMS, but its presence is here deduced from the optical emission of OH (Figure 6). We believe that this is due to the electron impact–driven dissociation of H_2O. The H and OH emissions are not equally strong due to different spectral properties. The process leading to strong H_α emission is similar to that observed before by Mucha et al. for diamond forming CH_4 discharges.[48]

4. Conclusions

Our work demonstrates that RF-ICP discharges can form syngas by DRM. Syngas yields of more than 70% were observed above 150 W at an equal feed CH_4/CO_2 ratio. Moreover, RF-ICP-driven reforming of mixed CO_2:CH_4 ratios demonstrates low energy costs comparable with APGD-driven DRM and much lower than DBD-driven DRM. By controlling the mixing ratios of CO_2:CH_4, we can tune up the yield of H_2 while minimizing the formation of C2 compounds. At high $CO_2/(CH_4 + CO_2)$ fractions in the feed, we observe significant amounts of H_α. The presence of H_α and OH in a RF-ICP-driven DRM process suppresses the recombination of CO + O, as the CO yields in DRM keep exceeding the CO yields found during the RF-ICP-driven discharge of pure CO_2. The formation of water plays a key role in the hydrogen atom recycling in an RF-ICP-driven DRM process. All in all, we show that DRM using RF-ICP is a promising alternative for transforming the greenhouse gases methane and CO_2 to valuable syngas under moderate conditions.

5. Experimental Section

All experiments were conducted in a designated RF-ICP reactor constructed in house (**Figure 8**). The plasma reactor consisted of a quartz tube, with a diameter of 40 mm and length of 600 mm. It was supported by two stainless steel flanges and sealed by O rings. The reactor tube was surrounded by a water-cooled copper coil. To establish efficient coupling of RF energy into the plasma, a matching box was placed between the RF power supply (13.56 MHz, 2 kW) and the copper coil. In contrast to our previous experiments, we could not mount a Langmuir probe to measure plasma parameters. A detailed technical description of the setup was published in previous studies.[20,49,50]

The maximum power used was 350 W, and the reflected power was maintained below 1 W by the matching box. However, this does not imply that all power from the supply was coupled into the plasma. Ohmic losses and RF losses by radiation will decrease the power actually coupled into the plasma. We had not optimized the coupling of power into plasma and only note that earlier work shows that very high coupling could be achieved.

The gases used in the reaction were directly obtained from gas cylinders and mixed before going into the reactor. Each gas cylinder was equipped with calibrated mass flow controllers (MFC, Sevenstar D07-19B) to set the flow. The plasma ignited inside the reactor tube, after supplying RF power. Prior to feeding the reaction gases, the reactor was evacuated to 1 Pa by a rotary pump with the nominal pumping speed around 18 L s^{-1}.

The light emitted by the plasma was collected by an optical fiber located 1.5 cm downstream from the coil, viewing the center of the reactor tube. The data were transmitted to our ultraviolet (UV)–vis–near-infrared (NIR)

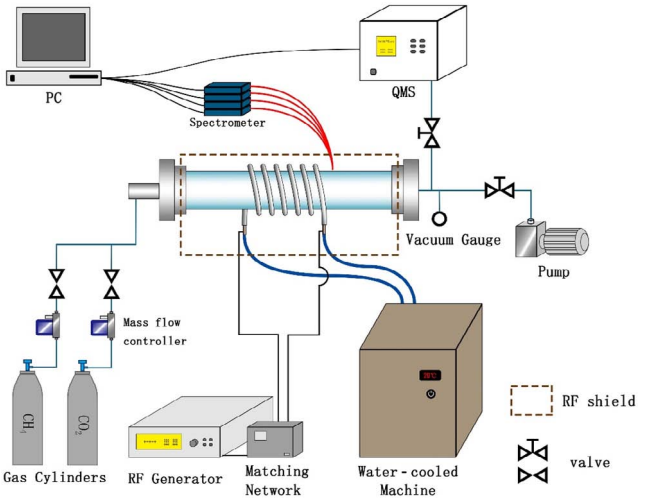

Figure 8. A schematic diagram of the experimental setup.

spectrometers (spectrometer, StellarNet LSR-NIR3b, LSR-UV2, LSR-VIS4b and LSR-VIS4). Data were analyzed as described earlier.[20]

To study the effect of the specific RF-ICP power supply and pressure on DRM, the experiments were carried out in different modes. First, at various power levels (from 0 to 150 W), the CH_4 or CO_2 flow was fixed at 50 sccm. Second, the power was maintained constant at 75 W, and the pressure was changed from 50 to 300 Pa at a total flow of 50 sccm. Third, we studied the effect of the feed gas composition. For that we modified the fraction $CO_2/(CH_4 + CO_2)$ while keeping the total feed gas rate and the power constant.

The composition of the gaseous products from the plasma reactor was determined by QMS. This was a powerful tool, because the gas composition could be measured in real time. In this way, the stability of the plasma can be checked continuously. Analyzing the mass spectra can be tricky, as different components led to ions with the same mass such as 28, and the sensitivity for each species could differ. Moreover, the transmission of the instrument may be mass dependent. To solve this, we used a simple approach to obtain the composition of the effluent gas. We determined the relative yields of equimolar mixtures of H_2, CH_4, CO, O_2 or CO_2, and Ar by QMS. The ratio of the yield of the parent molecular ions concerned and Ar^+ was used to determine the relative efficiency for each gas. This analysis yielded the relative composition of the product gas as a function of one of the experimental variables.

To deconvolute the contributions to for instance the mass 28 peak, we conducted an interpolation between extreme cases, where the composition was known, such as experiments with pure CO_2 or CH_4. In this interpolation we took the height of secondary peaks into consideration. The interpolation was done by hand on the basis of individual mass spectra. Intensities of C_2H_x species were hard to determine individually, also because of overlapping peaks in the mass spectrum. We obtained the C_2H_x signal by adding the intensities of the dominant peaks. QMS had internal consistency checks, namely, the H/C and O/C ratio of the measured intensities. The ratio was set by the reactant flow and could be changed by plasma action. For pure CH_4: $H/C = 4$ and for pure CO_2: $O/C = 2$. We checked that the analysis was done in a consistent way.

Previously, we reported the analysis data for the decomposition of pure CH_4 and pure CO_2 in this RF-ICP reactor setup.[20,49] Those studies form the basis for this work, which focused on pure methane and mixed CH_4/CO_2 reforming. Our calibration method was similar to the method described by Nguyen et al., where a fixed flow of argon flowed into the plasma reactor with a varying flow of the targeted gas species.[51] From the ratios of the partial pressure of argon and the targeted gas species together with the flow ratios of each gas, a calibration factor could be determined. With the calibration factor (i.e., the slope of the line), the ratio of partial pressures could be plotted now with the ratio of the flow rates of the gases for H_2, CO, CH_4, CO_2, and O_2. This linear extrapolation together with the extrapolation from data between steady-state gases that were activated by plasma (input power > 0) versus not activated by plasma (input power was 0 W) allowed us to determine the contribution to the mass 16 and mass 28 signals. From limiting cases, the composition of both mass 16 and mass 28 was then known, and we could make the distinction between the ions O^+ versus $CH_4{}^+$ and $C_2H_4{}^+$ versus CO^+.

Further the fragmentation pattern and fragmentation ratio of gas species like CH_4 and CO_2 are considered by a preliminary background scan. By taking a QMS background scan of CO_2, we identified and checked the fragmentation pattern and ratio of CO_2. This enabled us to check and correct the mass spectra on the amount of CO that originated from the fragmentation of the parent molecule CO_2 in the ionizer of the QMS.

The reproducibility of experimental runs was better than 20%. Within a single run, the signals for individual mass peaks reproduced to within 10% after stabilization of the system for a few minutes. The relative intensities of molecular C_2H_2, C_2H_4, and C_2H_6 could not be derived easily from mass spectrometry.[22,52,53] As this decomposition was not relevant for this study, we added the various contributions and gave a total signal of C_2H_x. The various molecules had different ionization cross sections, so we expected that there could be systematic errors up to 20% for the C_2H_x signal.

Acknowledgements

This work was supported by the National Natural Science Foundation of China (grant nos. 51561135013 and 21603202). The authors thank the Netherlands Scientific Organization (NWO) for the grant "Developing novel catalytic materials for converting CO_2, methane and ethane to high-value chemicals in a hybrid plasma-catalytic reactor" (China.15.119).

Conflict of Interest

The authors declare no conflict of interest.

Keywords

dry reforming of methane, optical emission spectroscopy, quadrupole mass spectrometry, radio frequency inductively coupled plasma, syngas

Received: July 24, 2019
Revised: February 17, 2020
Published online: March 5, 2020

[1] T. L. Frolicher, E. M. Fischer, N. Gruber, *Nature* **2018**, *560*, 360.
[2] J. D. Shakun, P. U. Clark, F. He, S. A. Marcott, A. C. Mix, Z. Y. Liu, B. Otto-Bliesner, A. Schmittner, E. Bard, *Nature* **2012**, *484*, 49.
[3] J. R. Malcolm, C. R. Liu, R. P. Neilson, L. Hansen, L. Hannah, *Conserv. Biol.* **2006**, *20*, 538.
[4] D. Hone, Sky: Meeting the Goals of the Paris Agreement, Shell International B.V., https://www.shell.com/energy-and-innovation/the-energy-future/scenarios/shell-scenario-sky.html, (accessed: August 2019).
[5] O. R. Inderwildi, S. J. Jenkins, D. A. King, *J. Phys. Chem. C* **2008**, *112*, 1305.
[6] D. Pakhare, J. Spivey, *Chem. Soc. Rev.* **2014**, *43*, 7813.
[7] J. L. Ewbank, L. Kovarik, C. C. Kenvin, C. Sievers, *Green Chem.* **2014**, *16*, 885.
[8] T. Stroud, T. J. Smith, E. Le Sache, J. L. Santos, M. A. Centeno, H. Arellano-Garcia, J. A. Odriozola, T. R. Reina, *Appl. Catal. B-Environ.* **2018**, *224*, 125.
[9] X. M. Tao, M. G. Bai, X. A. Li, H. L. Long, S. Y. Shang, Y. X. Yin, X. Y. Dai, *Prog. Energy Combust. Sci.* **2011**, *37*, 113.
[10] W. C. Chung, M. B. Chang, *Renew. Sust. Energ. Rev.* **2016**, *62*, 13.
[11] R. Snoeckx, A. Bogaerts, *Chem. Soc. Rev.* **2017**, *46*, 5805.
[12] A. H. Khoja, M. Tahir, N. A. S. Amin, *Energy Conv. Manag.* **2019**, *183*, 529.
[13] X. Tu, J. C. Whitehead, *Appl. Catal. B-Environ.* **2012**, *125*, 439.
[14] S. Ravasio, C. Cavallotti, *Chem. Eng. Sci.* **2012**, *84*, 580.
[15] A. H. Khoja, M. Tahir, N. A. S. Amin, *Int. J. Hydrog. Energy* **2019**, *44*, 11774.
[16] A. H. Khoja, M. Tahir, N. A. S. Amin, *Energy Conv. Manag.* **2017**, *144*, 262.
[17] S. Kameshima, K. Tamura, Y. Ishibashi, T. Nozaki, *Catal. Today* **2015**, *256*, 67.
[18] Y. X. Zeng, L. Wang, C. F. Wu, J. Q. Wang, B. X. Shen, X. Tu, *Appl. Catal. B-Environ.* **2018**, *224*, 469.
[19] D. Ray, D. Nepak, S. Janampelli, P. Goshal, C. Subrahmanyam, *Energy Technol.* **2019**, *7*, 11.
[20] D. Y. Zhang, Q. Huang, E. J. Devid, E. Schuler, N. R. Shiju, G. Rothenberg, G. van Rooij, R. L. Yang, K. Z. Liu, A. W. Kleyn, *J. Phys. Chem. C* **2018**, *122*, 19338.
[21] R. B. Piejak, V. A. Godyak, B. M. Alexandrovich, *Plasma Sources Sci. Technol.* **1992**, *1*, 179.

[22] M. Mozetic, A. Vesel, D. Alegre, F. L. Tabares, *J. Appl. Phys.* **2011**, *110*, 10.
[23] P. Patino, Y. Perez, M. Caetano, *Fuel* **2005**, *84*, 2008.
[24] Q. Chen, X. F. Yang, J. T. Sun, X. J. Zhang, X. G. Mao, Y. G. Ju, B. E. Koel, *Plasma Chem. Plasma Process.* **2017**, *37*, 1551.
[25] C. H. Tsai, T. H. Hsieh, *Ind. Eng. Chem. Res.* **2004**, *43*, 4043.
[26] K. Katayama, S. Fukada, M. Nishikawa, *Fusion Eng. Des.* **2010**, *85*, 1381.
[27] B. Jeon, E. D. Park, Y. K. Kim, *Res. Chem. Intermed.* **2018**, *44*, 3761.
[28] F. I. Bohrer, C. N. Colesniuc, J. Park, M. E. Ruidiaz, I. K. Schuller, A. C. Kummel, W. C. Trogler, *J. Am. Chem. Soc.* **2009**, *131*, 478.
[29] C. S. Shen, D. K. Sun, H. S. Yang, *J. Nat. Gas Chem.* **2011**, *20*, 449.
[30] Q. Chen, J. T. Sun, X. J. Zhang, *Chin. J. Chem. Eng.* **2018**, *26*, 1041.
[31] P. Chawdhury, D. Ray, D. Nepak, C. Subrahmanyam, *J. Phys. D-Appl. Phys.* **2019**, *52*, 11.
[32] L. Wang, Y. H. Yi, C. F. Wu, H. C. Guo, X. Tu, *Angew. Chem. Int. Ed.* **2017**, *56*, 13679.
[33] H. Singh, D. B. Graves, *J. Appl. Phys.* **2000**, *88*, 3889.
[34] D. H. Li, X. Li, M. G. Bai, X. M. Tao, S. Y. Shang, X. Y. Dai, Y. X. Yin, *Int. J. Hydrog. Energy* **2009**, *34*, 308.
[35] Y. Xu, Q. Wei, H. L. Long, X. Q. Zhang, S. Y. Shang, X. Y. Dai, Y. X. Yin, *Int. J. Hydrog. Energy* **2013**, *38*, 1384.
[36] H. L. Long, S. Y. Shang, X. M. Tao, Y. P. Yin, X. Y. Dai, *Int. J. Hydrog. Energy* **2008**, *33*, 5510.
[37] R. Snoeckx, Y. X. Zeng, X. Tu, A. Bogaerts, *RSC Adv.* **2015**, *5*, 29799.
[38] Y. P. Zhang, Y. Li, Y. Wang, C. J. Liu, B. Eliasson, *Fuel Process. Technol.* **2003**, *83*, 101.
[39] A. J. Zhang, A. M. Zhu, J. Guo, Y. Xu, C. Shi, *Chem. Eng. J.* **2010**, *156*, 601.
[40] A. M. Huang, G. G. Xia, J. Y. Wang, S. L. Suib, Y. Hayashi, H. Matsumoto, *J. Catal.* **2000**, *189*, 349.
[41] Q. Chen, W. Dai, X. M. Tao, H. Yu, X. Y. Dai, Y. X. Yin, *Plasma Sci. Technol.* **2006**, *8*, 181.
[42] A. J. Wu, J. H. Yan, H. Zhang, M. Zhang, C. M. Du, X. D. Li, *Int. J. Hydrog. Energy* **2014**, *39*, 17656.
[43] M. W. Li, G. H. Xu, Y. L. Tian, L. Chen, H. F. Fu, *J. Phys. Chem. A* **2004**, *108*, 1687.
[44] V. Shapoval, E. Marotta, *Plasma Process. Polym.* **2015**, *12*, 808.
[45] P. Liu, X. S. Liu, J. Shen, Y. X. Yin, T. Yang, Q. Huang, D. Auerbach, A. W. Kleiyn, *Plasma Sci. Technol.* **2019**, *21*, 4.
[46] T. Yang, J. Shen, T. C. Ran, J. Li, P. Chen, Y. X. Yin, *Plasma Sci. Technol.* **2018**, *20*, 9.
[47] J. Li, X. Q. Zhang, J. Shen, T. C. Ran, P. Chen, Y. X. Yin, *J. CO2 Util.* **2017**, *21*, 72.
[48] J. A. Mucha, D. L. Flamm, D. E. Ibbotson, *J. Appl. Phys.* **1989**, *65*, 3448.
[49] Q. Huang, D. Y. Zhang, D. P. Wang, K. Z. Liu, A. W. Kleyn, *J. Phys. D Appl. Phys.* **2017**, *50*, 6.
[50] R. L. Yang, D. Y. Zhang, K. W. Zhu, H. L. Zhou, X. Q. Ye, A. W. Kleyn, Y. Hu, Q. Huang, *Acta Phys. Chim. Sin.* **2019**, *35*, 292.
[51] S. V. T. Nguyen, J. E. Foster, A. D. Gallimore, *Rev. Sci. Instrum.* **2009**, *80*, 8.
[52] F. L. Tabares, D. Alegre, M. Mozetk, A. Vesel, *Nukleonika* **2012**, *57*, 287.
[53] X. Cao, Y. Xia, B. Chen, S. Tian, C. Wang, D. Yang, X. Xue, W. Zhang, J. Wang, F. Gou, Z. Zhu, W. Ou, S. Chen, *Plasma Sci. Technol.* **2015**, *17*, 20.